Electronic Supplementary Material (ESI) for Dalton Transactions.
This journal is © The Royal Society of Chemistry 2021

Supporting Information

Design, synthesis, structural, spectral, redox properties and phenoxazinone synthase activity of tripodal pentacoordinate Mn(II) complexes with impressive turnover numbers

Figure captions

Fig. S1 X-ray crystal structures of the non-equivalent cations in the asymmetric unit of the crystals of **1** and **2** respectively; Ellipsoids are drawn with 50% probability. Hydrogen atoms and counter anions are omitted for better clarity.

Fig. S2 ESI-MS spectra of (a) **1** and (b) simulated mass spectra.

Fig. S3 ESI-MS spectra of (a) **2** and (b) simulated mass spectra.

Fig. S4 ^{1}H NMR spectra of $\mathbf{L^2}$ in $(CD_3)_2SO$ in room temperature.

Fig. S5 FT-IR (solid) spectra of (a) $\mathbf{L^1}$, (b) $\mathbf{L^2}$, (c) **1** and (d) **2** respectively.

Fig. S6 Cyclic voltammograms (black) and differential pulse voltammograms (red) for **1** (left) and **2** (right) in dry DMF using 0.1 M TBAP as supporting electrolyte versus SCE, CV scan rate 100 mV s^{-1}.

Fig. S7 *o*-aminophenol oxidation in methanol by **2**.

Fig. S8 Increase in phenoxazinone absorbance during the catalytic oxidation of *o*-aminophenol (a) 0.25×10^{-2} M, (b) 0.5×10^{-2} M, (c) 0.75×10^{-2} M and (d) 1.0×10^{-2} M in the presence of complex **1** (left) and respective rate constant determination (right).

Fig. S9 Increase in phenoxazinone absorbance during the catalytic oxidation of *o*-aminophenol (a) 0.1×10^{-2} M, (b) 0.3×10^{-2} M, (c) 0.5×10^{-2} M and (d) 1.0×10^{-2} M in the presence of complex **2** (left) and respective rate constant determination (right).

Fig. S10 Initial rate versus substrate concentration plot for the oxidation of *o*-aminophenol catalyzed by **2**.

Fig. S11 Lineweaver-Burk plots for the oxidation of *o*-aminophenol catalyzed by **2**.

Fig. S12 Evidence of adduct formation found *via* mass spectrometry (a) and (c) for **1** and **2** with their simulated mass spectra (b) and (d).

Fig. S13 Evidence of peroxide attachment found *via* mass spectrometry (a) and (c) for **1** and **2** with their simulated mass spectra (b) and (d).

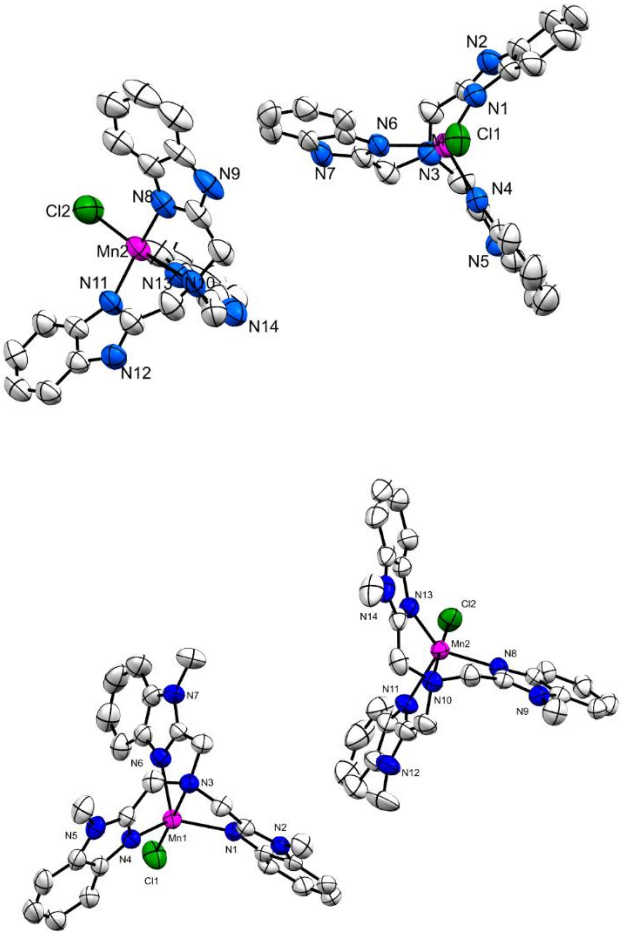

Fig. S1 X-ray crystal structures of the non-equivalent cations in the asymmetric unit of the crystals of **1** and **2** respectively; Ellipsoids are drawn with 50% probability. Hydrogen atoms and counter anions are omitted for better clarity.

(a)

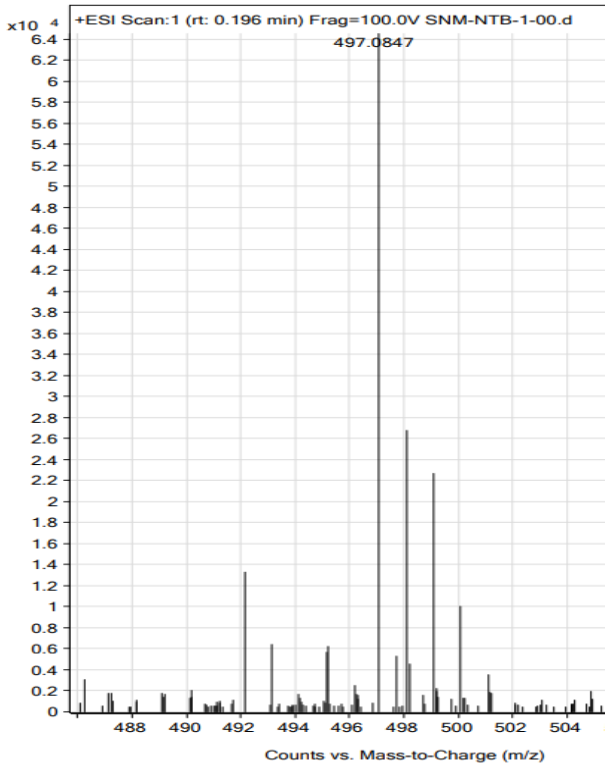

(b)

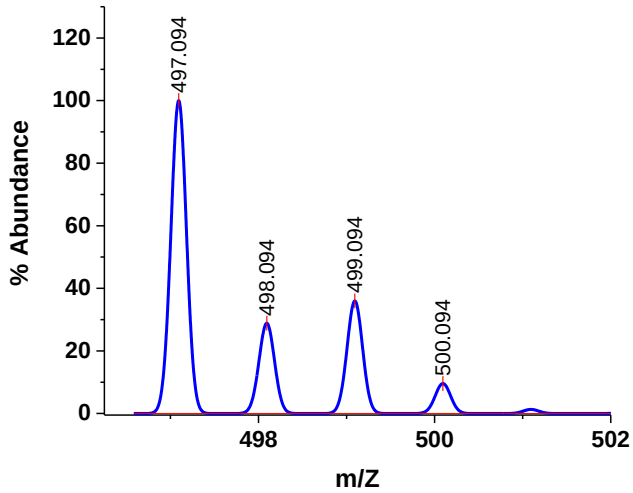

Fig. S2 ESI-MS spectra of (a) **1** and (b) simulated mass spectra.

(a)

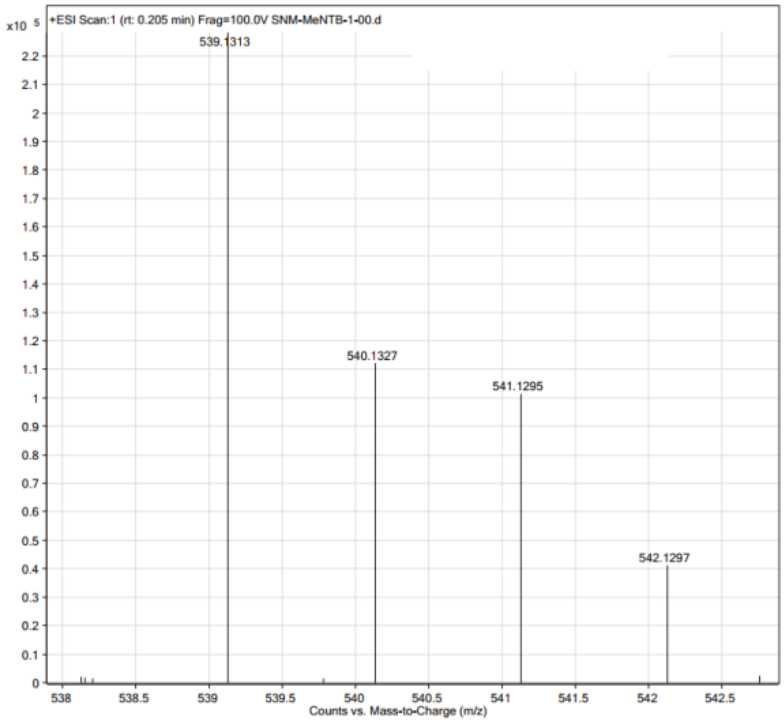

(b)

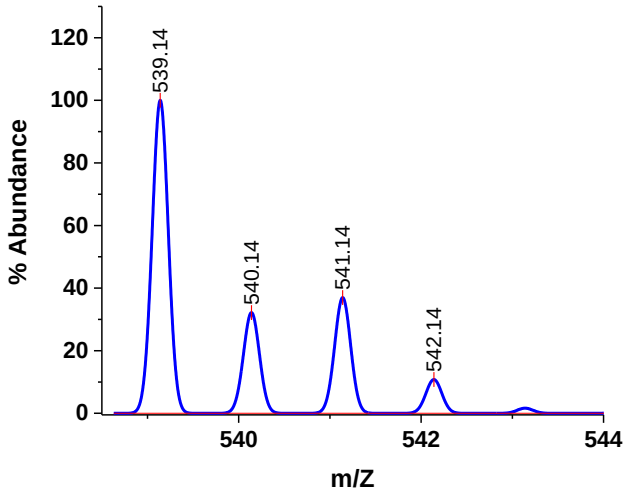

Fig. S3 ESI-MS spectra of (a) **2** and (b) simulated mass spectra.

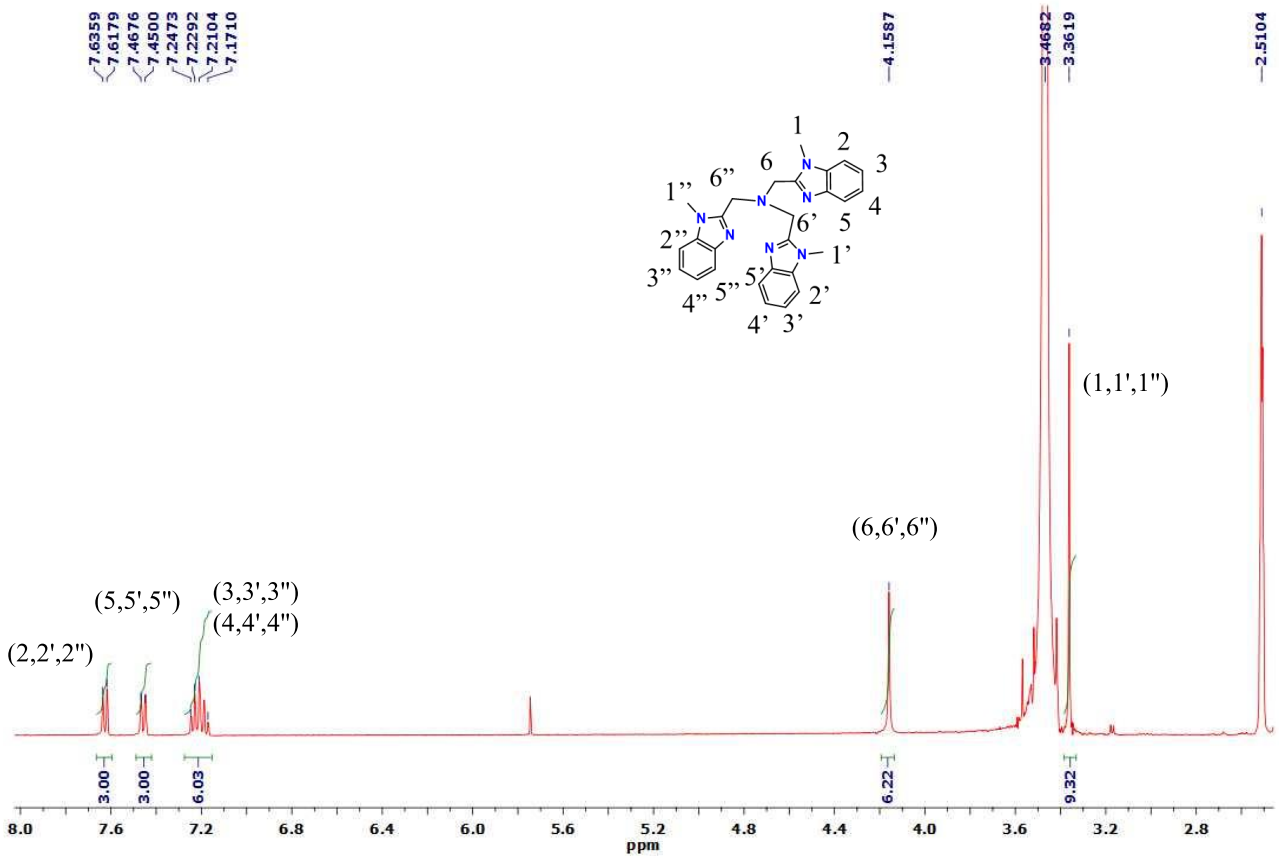

Fig. S4 ^{1}H NMR spectra of **L^{2}** in DMSO-d^{6} in room temperature

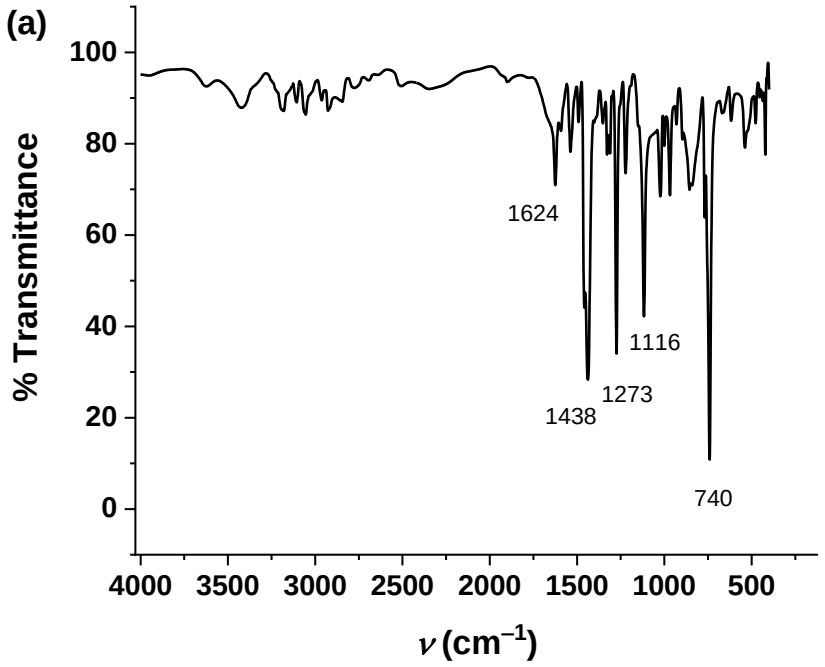
(a)
% Transmittance
100
80
60
40
20
0
1624
1438
1273
1116
740
4000
3500
3000
2500
2000
1500
1000
500
ν (cm−1)

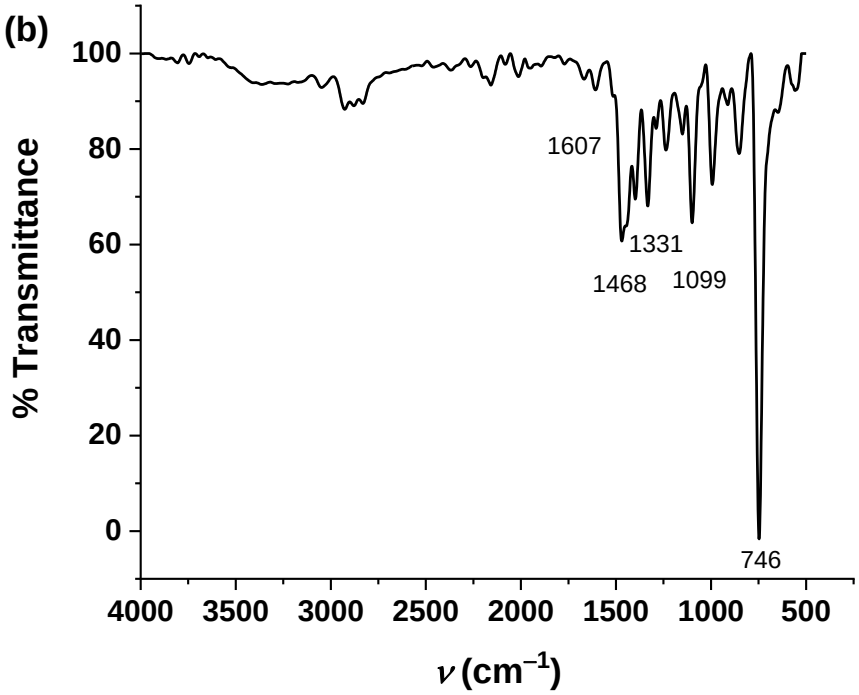
(b)
% Transmittance
100
80
60
40
20
0
1607
1468
1331
1099
746
4000
3500
3000
2500
2000
1500
1000
500
ν (cm−1)

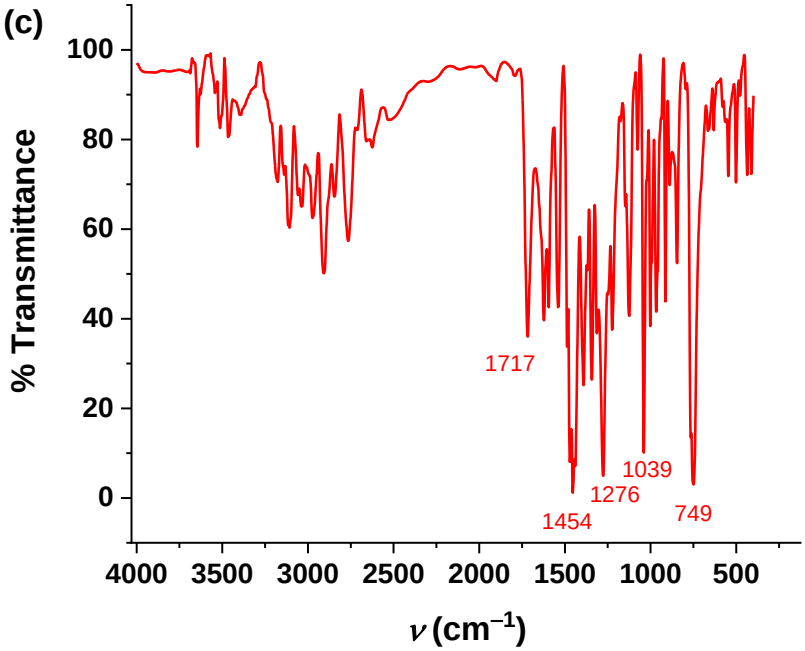

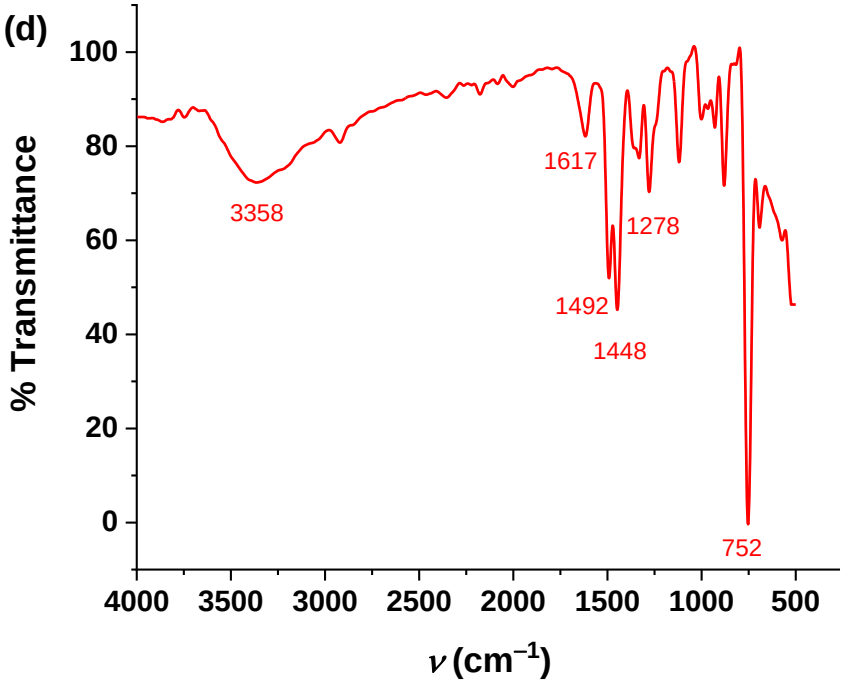

Fig. S5 FT-IR (solid) spectra of (a) $\mathbf{L^1}$, (b) $\mathbf{L^2}$, (c) **1** and (d) **2** respectively.

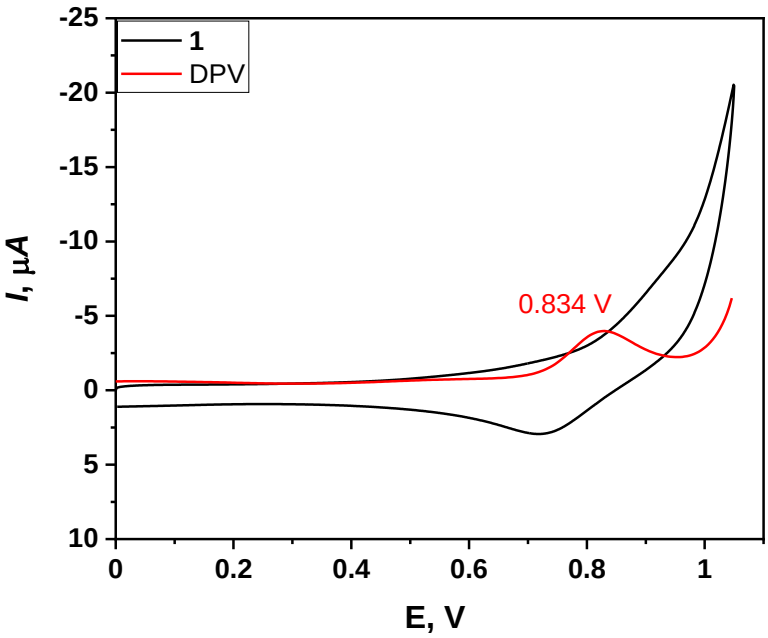

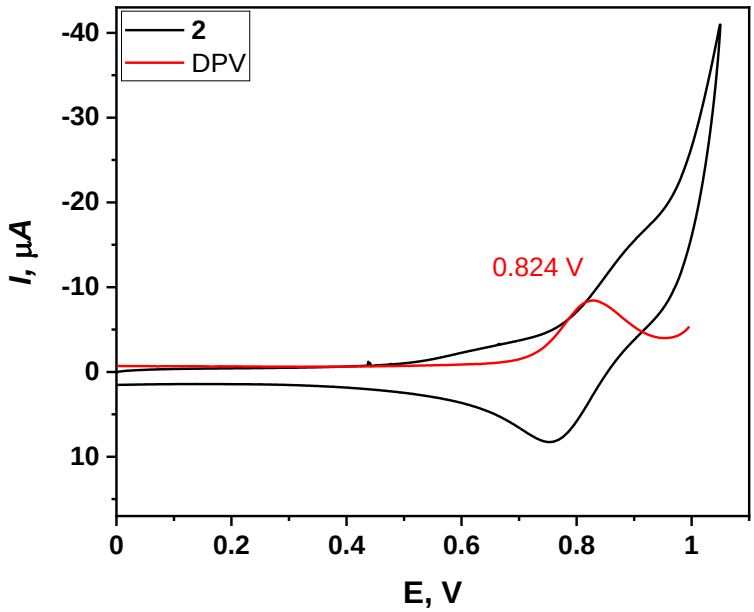

Fig. S6 Cyclic voltammograms (black) and differential pulse voltammograms (red) for **1** (up) and **2** (down) in dry DMF using 0.1 M TBAP as supporting electrolyte versus SCE, CV scan rate 100 mV s^{-1}.

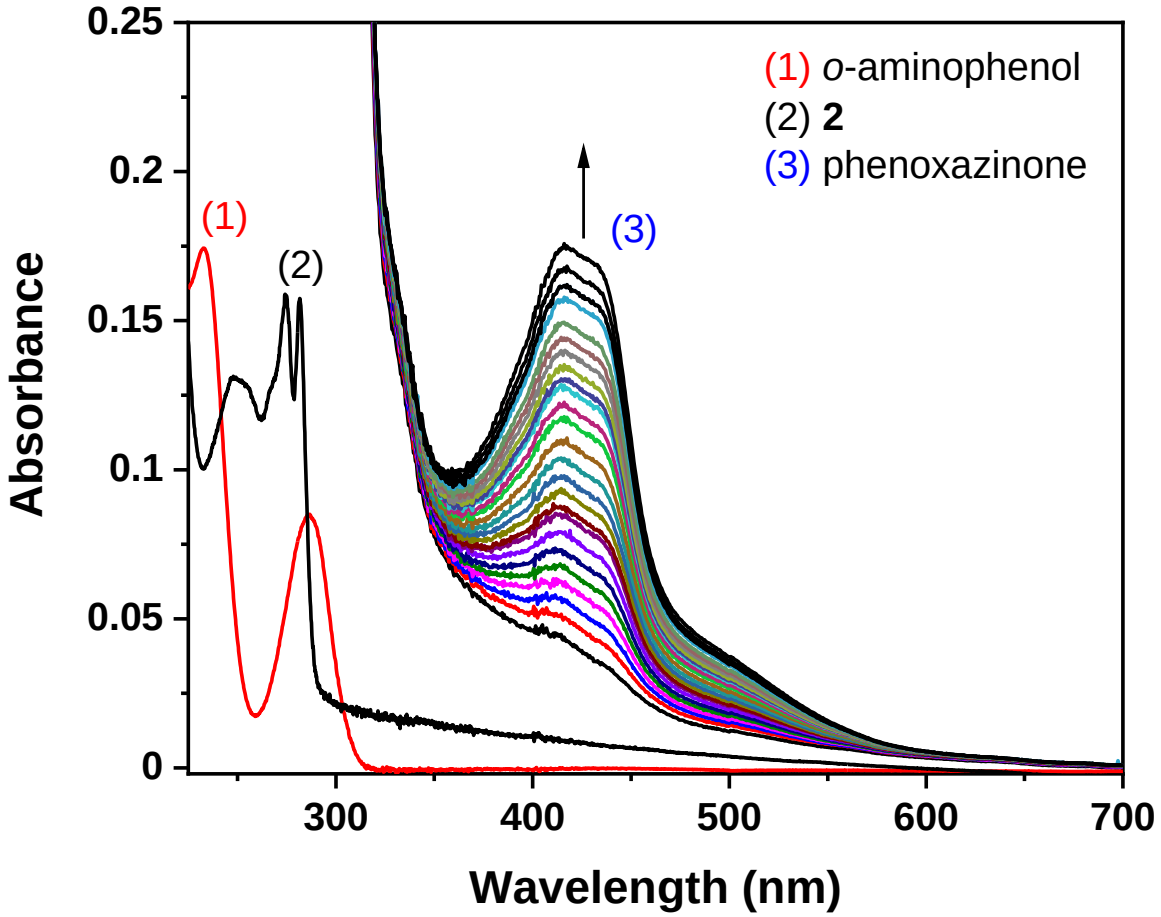

Fig. S7 *o*-aminophenol oxidation in methanol by **2**.

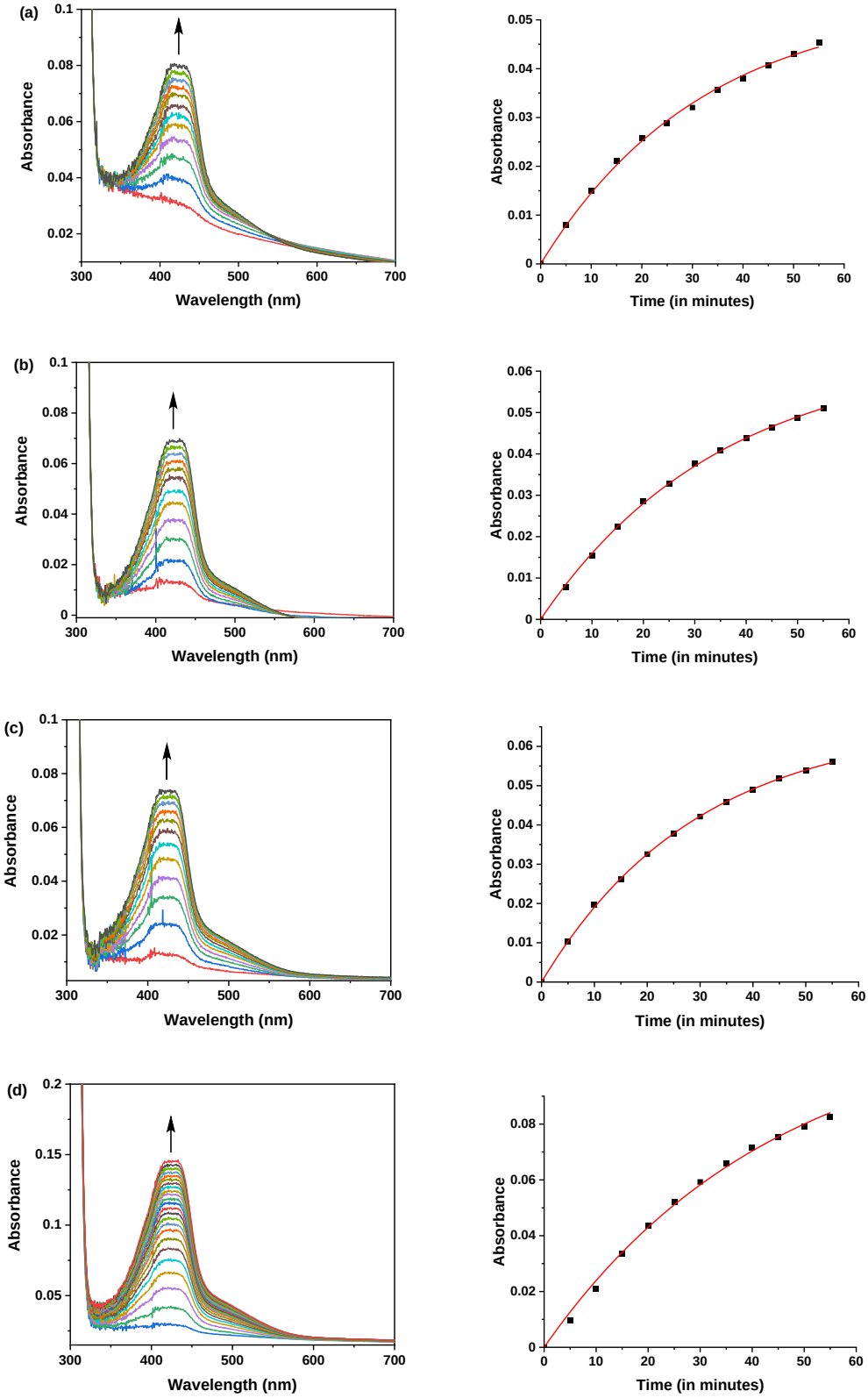

Fig. S8 Increase in phenoxazinone absorbance during the catalytic oxidation of *o*-aminophenol (a) 0.25×10^{-2} M, (b) 0.5×10^{-2} M, (c) 0.75×10^{-2} M and (d) 1.0×10^{-2} M in the presence of complex **1** (left) and respective rate constant determination (right).

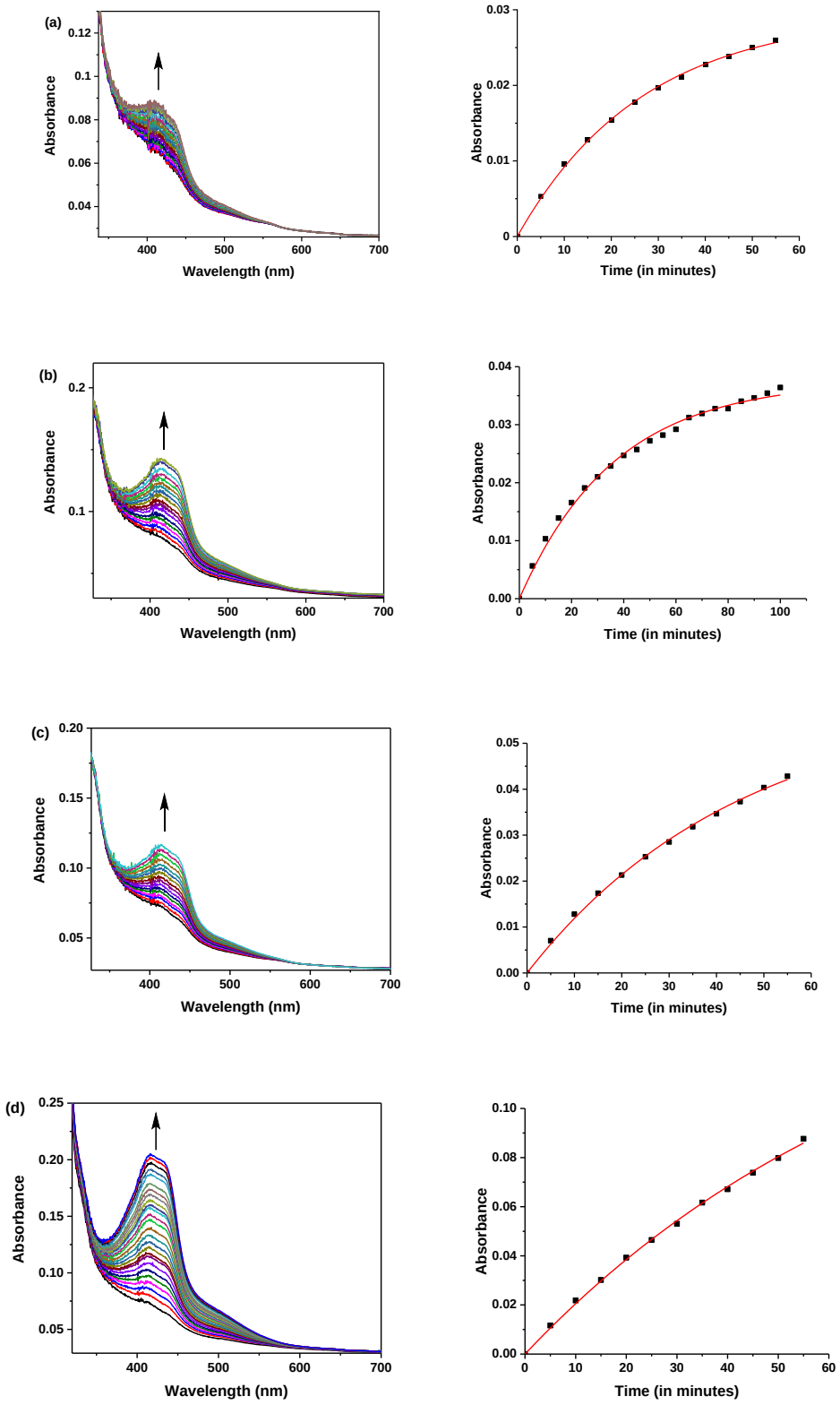

Fig. S9 Increase in phenoxazinone absorbance during the catalytic oxidation of *o*-aminophenol (a) 0.1×10^{-2} M, (b) 0.3×10^{-2} M, (c) 0.5×10^{-2} M and (d) 1.0×10^{-2} M in the presence of complex **2** (left) and respective rate constant determination (right).

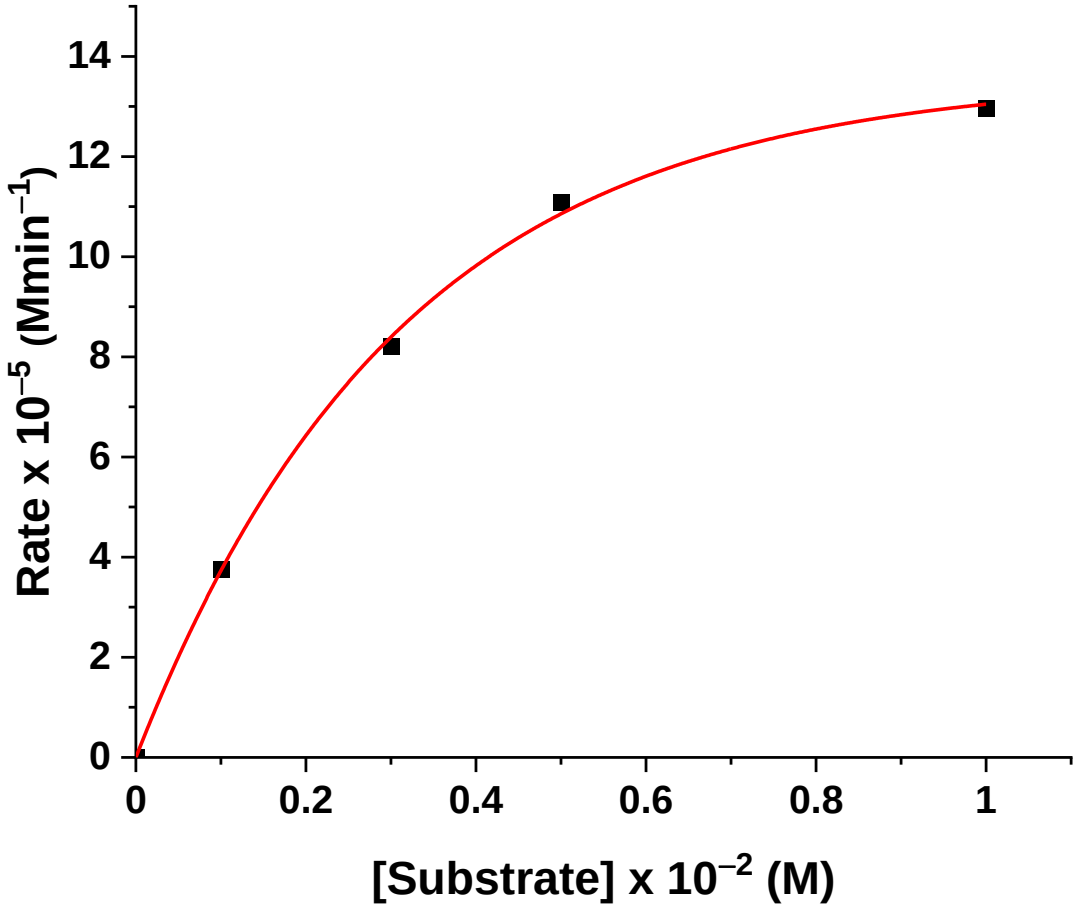

Fig. S10 Initial rate versus substrate concentration plot for the oxidation of *o*-aminophenol catalyzed by **2**.

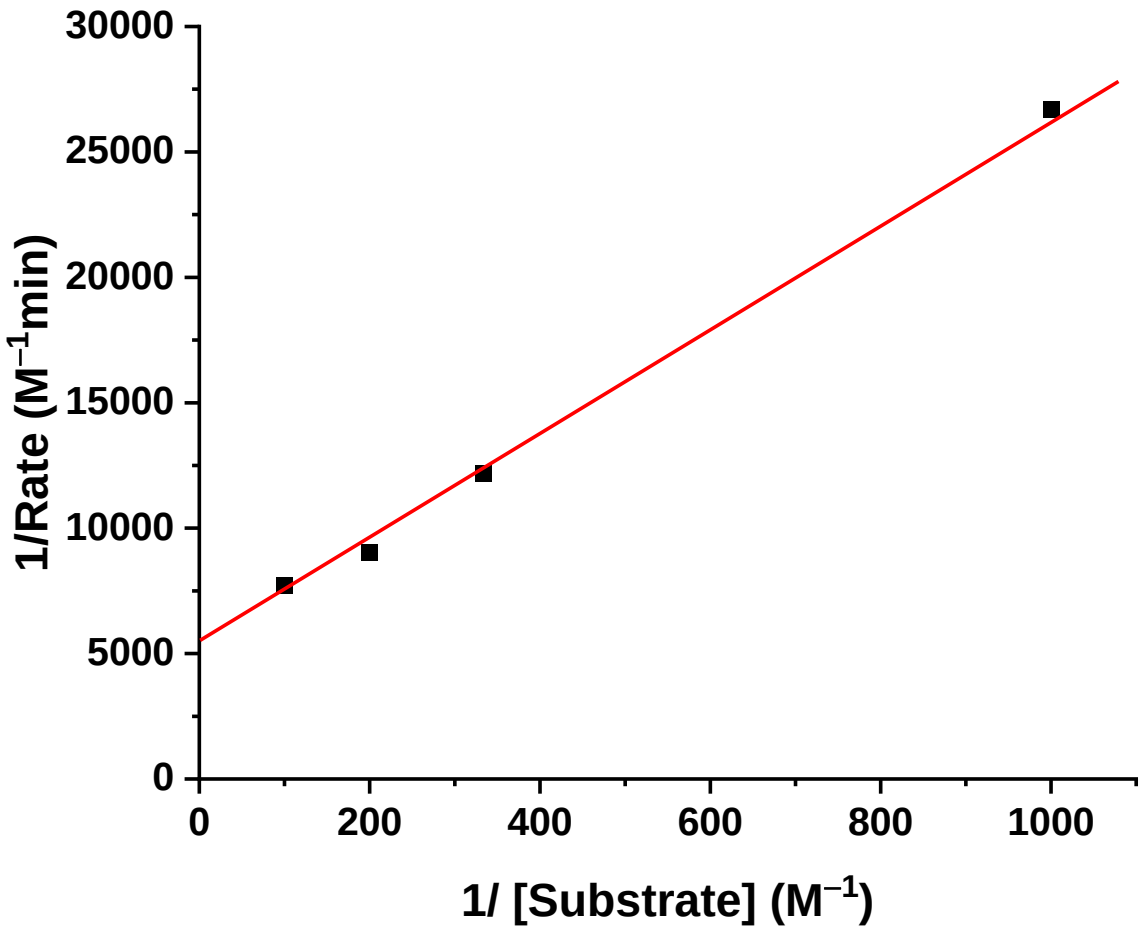

Fig. S11 Lineweaver-Burk plots for the oxidation of *o*-aminophenol catalyzed by **2**.

(a)

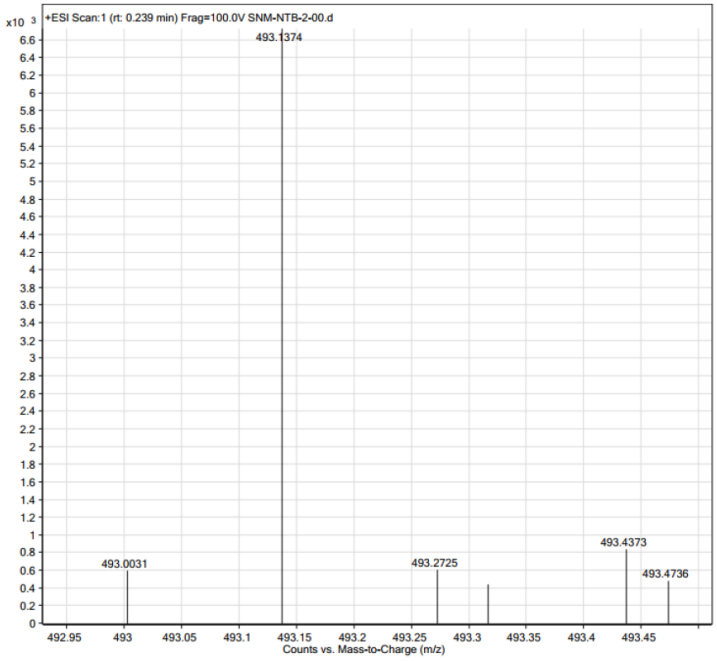
+ESI Scan:1 (rt: 0.239 min) Frag=100.0V SNM-NTB-2-00.d
x10 3
493.1374
493.0031
493.2725
493.4373
493.4736
Counts vs. Mass-to-Charge (m/z)

(b)

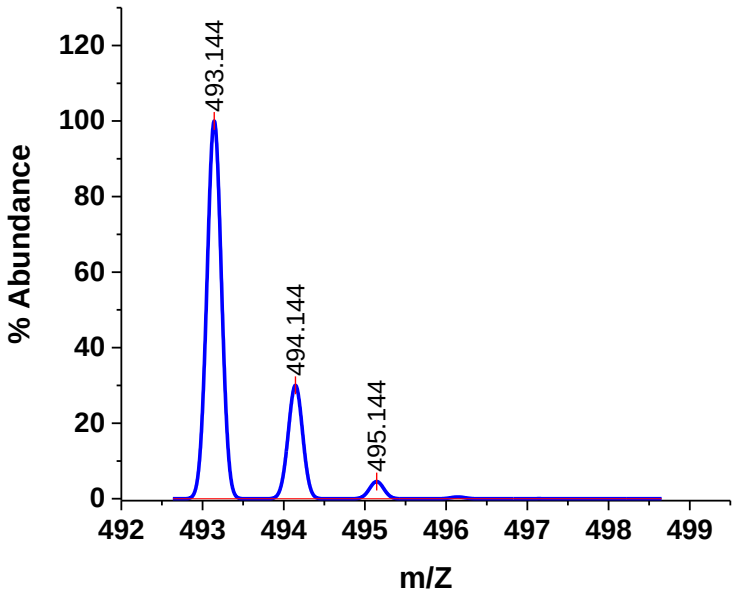
% Abundance
m/Z
493.144
494.144
495.144

(c)

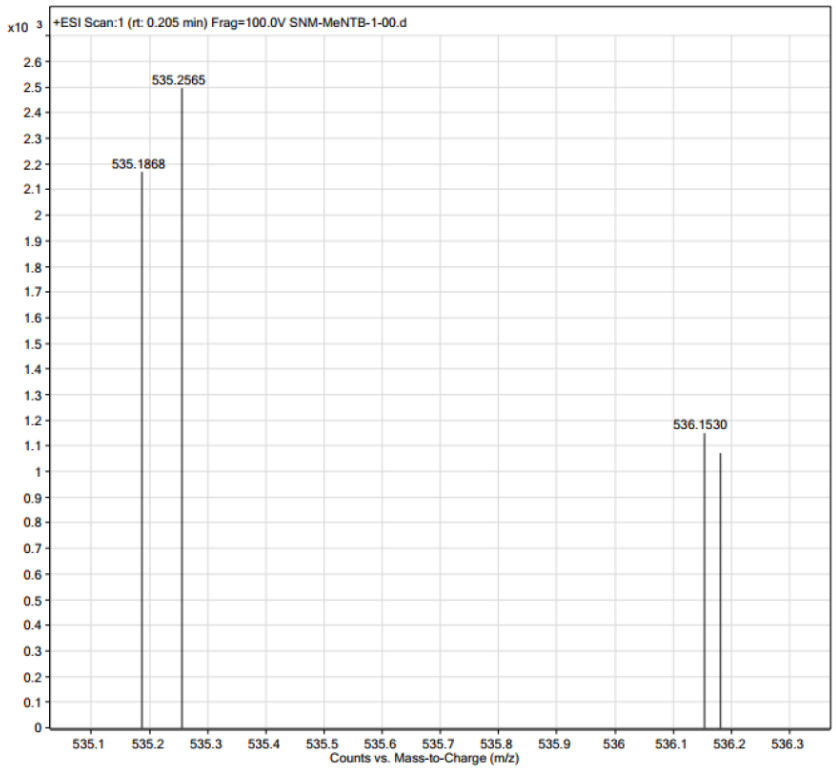

(d)

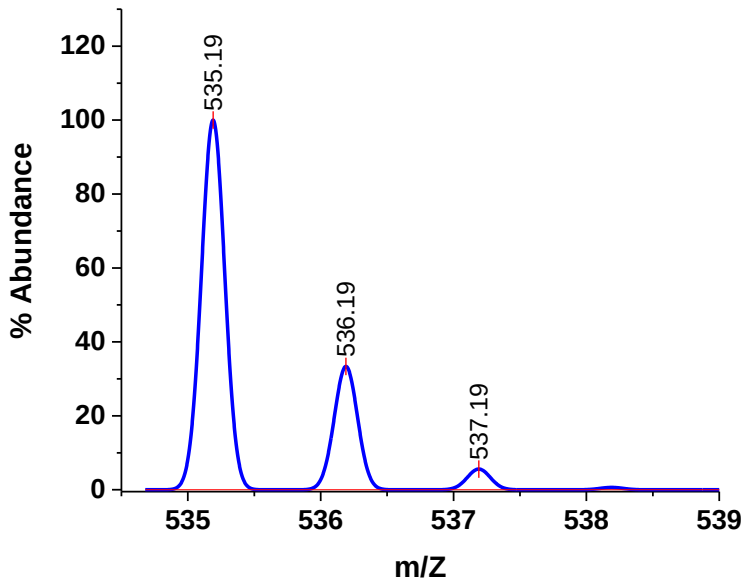

Fig. S12 Evidence of adduct formation found *via* mass spectrometry (a) and (c) for **1** and **2** with their simulated mass spectra (b) and (d).

(a)

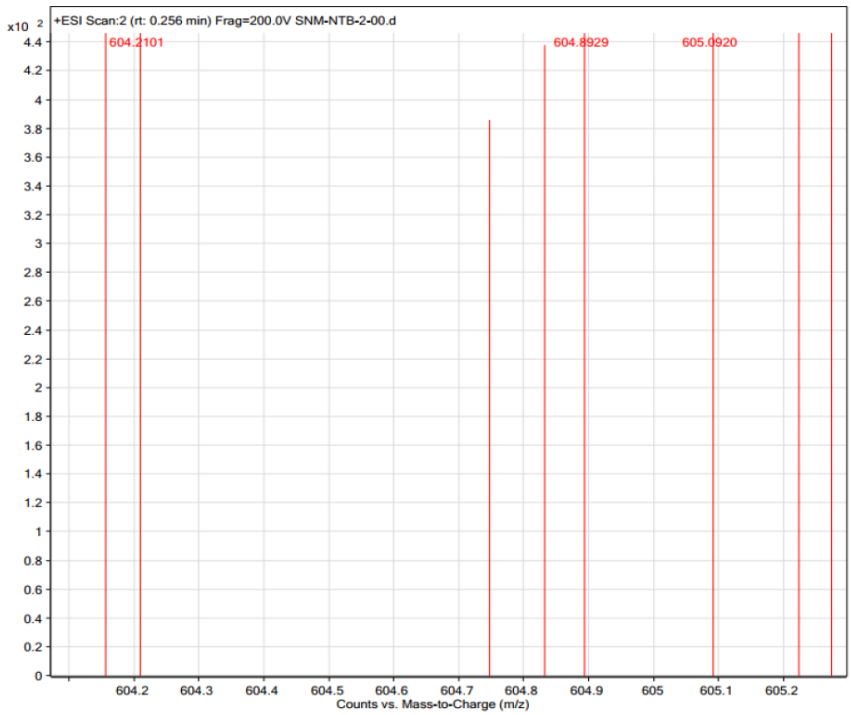
+ESI Scan:2 (rt: 0.256 min) Frag=200.0V SNM-NTB-2-00.d
x10 2
604.2101
604.8929
605.0920
Counts vs. Mass-to-Charge (m/z)

(b)

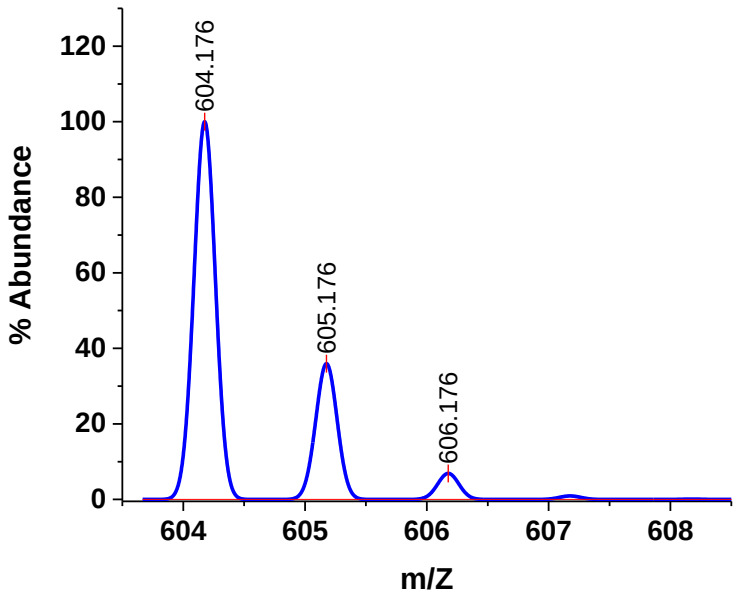
% Abundance
m/Z
604.176
605.176
606.176

(c)

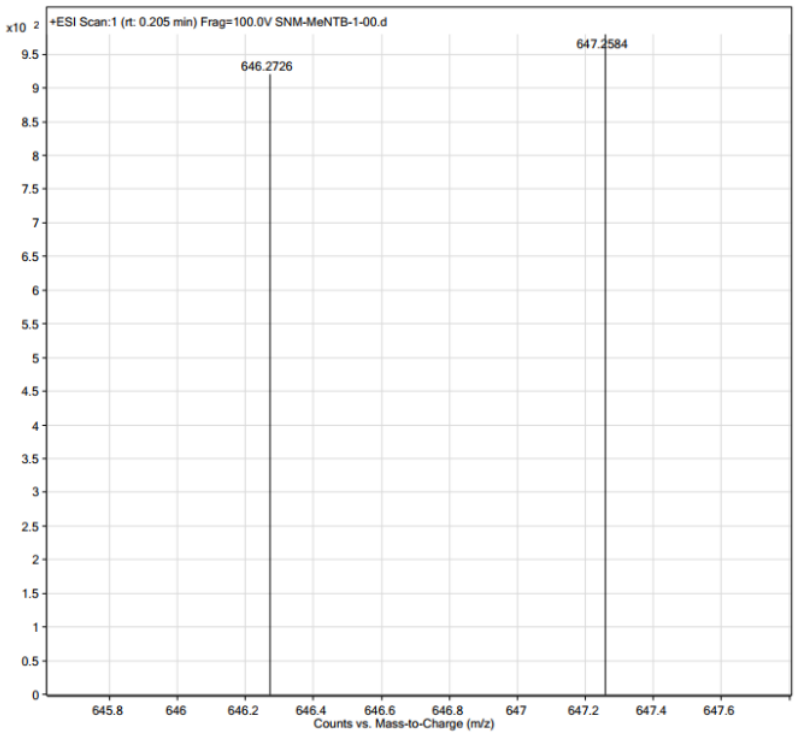

(d)

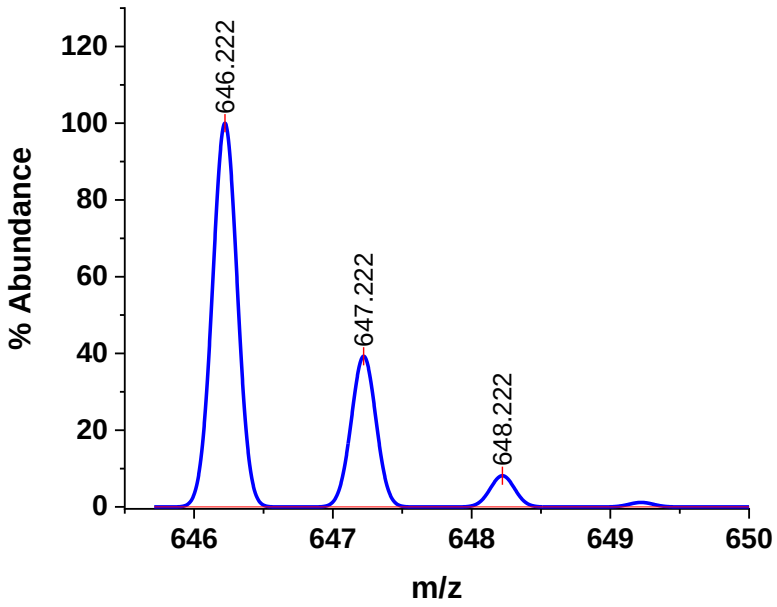

Fig. S13 Evidence of peroxide attachment found *via* mass spectrometry (a) and (c) for **1** and **2** with their simulated mass spectra (b) and (d).